Available online at www.sciencedirect.com
SCIENCE DIRECT
Polymer 46 (2005) 3895–3905
polymer
www.elsevier.com/locate/polymer

Mechanical properties of short fiber reinforced thermoplastic blends

Plamen G. Malchev[a,b,*], Ciprian T. David[c], Stephen J. Picken[a,b], Alexandros D. Gotsis[a,b,1]

[a]Department of Polymer Materials and Engineering, Delft University of Technology, Julianalaan 136, 2628 BL Delft, The Netherlands
[b]Dutch Polymer Institute, P.O. Box 902, 5600 AX Eindhoven, The Netherlands
[c]Materials Science and Engineering Faculty, Transilvania University of Brasov, Str. Colina Universitatii 1, 2200 Brasov, Romania

Received 14 October 2004; received in revised form 28 January 2005; accepted 4 February 2005
Available online 1 April 2005

Abstract

An immiscible thermoplastic component was added to a conventional short fiber reinforced polymer to study its effect on the mechanical properties of the composite. Because of the preferential wetting of the fiber reinforcement a continuous network was formed of fibers 'welded' together by the minor component within the matrix polymer.

Polyethylene (PE) was used as the matrix, polyamide-6 (PA6) as dispersed polymer phase and glass fibers (GF) as reinforcement. The obtained composite retained unusually high values of the elasticity modulus at temperatures above the melting point of the matrix. The upper limit of the 'applicability' of the material is determined by the melting point of the minor component. A simple model was derived to describe the mechanical properties of the composite. The model shows a good agreement with the experimental data. The influence of the model parameters on the predictions of the model was examined.

Keywords: Short fiber reinforced blend; Preferential wetting; Fiber network

1. Introduction

Polymer blending and reinforcement has been studied for many years (e.g. Refs. [1,2]). Most studies involved blends or composites with two components. Recently three- (and more) phase polymer composites have also attracted the attention of scientific research and the interest of the industry. These are studied in an effort to design materials with novel properties or to improve already existing ones. One of the first papers in this area is the work of Xanthos and Narh, [3]. The paper discussed the possibility to recycle different industrial waste streams of thermoplastic blends by the addition of a fiber reinforcement. The glass fiber reinforcing improved the mechanical properties of the blends enough to be used as a replacement material for pure thermoplastics. An example of a product design based on such a composite was also described. Studies devoted to the development of electrically conductive three-phase polymer composites comprise another direction of the research in the area, e.g. Ref. [4]. Most of the efforts aim to reduce the amount of the electrically conductive phase (most often carbon black (CB)) by controlling the morphology of the blends and to facilitate, thus, processing of the material. Rather high conductivities at very low CB content were found when the CB phase was localized preferentially at the interface between the two polymeric components or in the minor component. This was due to a 'double percolation' effect. A few articles studying exclusively the mechanical properties of three-phase polymer composites have also become available recently [5–7].

The present article is concerned with the improvement of the mechanical properties of glass fiber reinforced polymers. It investigates the possibility to extend the properties of conventional short fiber reinforced thermoplastics by adding minor quantities of a second immiscible thermoplastic polymer. Depending on the mixing conditions and the properties of the polymeric phases and the fiber reinforcement, an effective network of fibers can be formed within the matrix polymer. This network will consist of

* Corresponding author. Address: Department of Polymer Materials and Engineering, Delft University of Technology, Julianalaan 136, 2628 BL Delft, The Netherlands. Tel.: +31 15 2784603; fax: +31 15 2787415.
E-mail address: p.g.malchev@tnw.tudelft.nl (P.G. Malchev).
[1] Present address: Department of Sciences, Technical University of Crete, 73100 Chania, Greece.

0032-3861/$ - see front matter © 2005 Elsevier Ltd. All rights reserved.
doi:10.1016/j.polymer.2005.02.091

glass fibers welded together by the minor polymeric component. The formation of the network, generally, leads to the enhancement of the mechanical properties of the composite.

The mechanical properties of such a ternary composite, therefore, are determined not only by the properties of the constituent fibers and matrix, and by their volume fractions, but also by the state of the formed network. The parameters of the network structure that should have an influence on the mechanical properties of the composite include the average orientation of the fibers within the network with respect to the direction of the externally applied test force, the number or density of junction points, and their strength and torsional stiffness. In turn, these are also dependent on the amount of the welding minor phase that participates in the network and the mechanical properties of this phase.

Since, the formation of the network is driven by the preferential wetting of the fibers by the minor polymeric phase, one expects that the interfacial properties of the three components will indirectly influence the mechanical properties of the composite. This is studied qualitatively here by changing the compatibility between the fiber reinforcement and the matrix. The viscosities of the two polymer melts are also expected to have an influence (e.g. Refs. [1,8]), since their ratio may determine how fine the dispersion of the minor polymeric component will be. However, in the present work it is found that the interfacial tensions, indeed, have a dominant influence on the mechanical properties, while the viscosities do not strongly affect the structure of the formed network, at least, for the mixers and at the mixing conditions that were applied.

The mechanical properties of the manufactured three-phase composites are characterized by dynamic mechanical testing. The well known mechanical models developed for two-component systems (e.g. as proposed by Ref. [9]) are, however, difficult to apply for the investigated three-phase system and, generally, failed to describe the mechanical data in the whole measured temperature region. Therefore, another simple theoretical model is proposed in Section 4 of the present paper. The model is based on the observed morphology for the three-phase systems and uses the mechanical properties of the constituent phases as input data. Many comprehensive models for the mechanical properties of composites include random distribution of the reinforcing fibers (e.g. Refs. [10–14]). In the present work a representative unit block is introduced to describe the geometry of the network. Three elementary modes of deformation of the block are then considered: twisting of a network junction point, bending of the fiber reinforcement between two junction points and stretching of the fibers. These elementary deformation modes cover all possible deformations in a fiber network and are commonly discussed when the mechanical properties of the networks are described. This is a more complete approach than the one followed by Refs. [12–14], where only stretching and bending of the fibers was cosidered and the junction points were regarded as rigid (no twist). The model proposed in the present article calculates the composite modulus by minimizing the total deformation energy. Its 'adjustable' parameters are identified and are dependent on the morphology. The successful description of the measured experimental data by the model is remarkable, considering its simplicity.

2. Materials and measuring techniques

Two low density polyethylene grades with different viscosities (PE1 and PE2) and a polyamide-6 (PA6) were used as matrix and dispersed phase, respectively. These two polymers are totally immiscible at the temperature where the blending process took place. Short glass fibers compatible with either PA6 or PE were used for the reinforcement: GF1 and GF2, respectively. The physical properties of the materials are summarized in Table 1. Except for the PA6 component, which was dried prior to use in a vacuum oven at 80 °C for at least 24 h, the other components were used as delivered.

In order to test the concept of the network formation, several binary and ternary composites (of different constituents and different component volume fractions) have been blended in a Collin single-screw extruder. A mixing screw with square pitch was used. The diameter was 20 mm and the extruder has a *L*/*D* ratio of 24, it was operated at 60 rpm at 240 °C (at the mixing element) for all blends. At this temperature both polymeric components were in the melt state. Using microscopy the homogeneity of the samples was found to be satisfactory.

The different binary and ternary mixtures that were compounded are denoted in the present article by the volume fraction of the components (in %) followed by the notation of the components themselves. For example, 95/05 PE1/GF1 and 84/16 PE1/PA6 are codes for binary mixtures; 85/05/10 PE1/PA6/GF2 is the code for a ternary mixture. In the last example the content of PE is 85 vol%, the content of PA6 is 5 vol% and the content of GF is 10 vol%; the particular PE and GF used are PE1: Stamylan LD2102 and GF2: PPG 3299 (Table 1).

The samples for the mechanical tests were punched out of a plate that was made by hot press consolidation of the extrudates at a temperature of 260 °C for about 10 min, while also trying to conserve the orientation of the extrudates. The dimensions of all samples were approximately $2\times2.5\times10\ \mathrm{mm}^3$, with the longest side parallel to the direction of the extrusion.

The dynamic mechanical properties were measured in a Perkin–Elmer Dynamic Mechanical Analyzer (DMA 7e), in tensile mode. The device applies a continuous sinusoidal oscillatory deformation on the sample and measures the force required to produce a specific oscillation amplitude. The moduli are derived from the value of this force and its phase difference with respect to the deformation. These are

Table 1
Physical properties of the initial materials

	Polymers			Glass fibers	
Code	PA6	PE1	PE2	GF1	GF2
Trade name	Akulon K222D	Stamylan LD2102	Stamylan LD2100	PPG 3545	PPG 3299
Melt flow rate	–	1.9 dg/min	0.3 dg/min	–	–
Diameter	–	–	–	10.0 μm	13.7 μm
Length	–	–	–	4.5 mm	3.0 mm
Compatible *w*	–	–	–	PA6	PE
Density	1.13 g/cm^3	0.921 g/cm^3	0.921 g/cm^3	2.60 g/cm^3	2.60 g/cm^3
E modulus	2 GPa (25 °C)	250 MPa (25 °C)	250 MPa (25 °C)	72 GPa (25 °C)	72 GPa (25 °C)
Melting temperature	220 °C	110 °C	110 °C	–	–

The polymers are commercial grades and were delivered by DSM. The glass fibers were delivered by PPG Industries.

the elastic (in-phase, storage), E', and viscous (out-of-phase, loss), E'', terms of the complex dynamic tensile modulus of a viscoelastic material.

The temperature of the measurements was raised in the present experiments at a constant rate of 5 °C/min, from 25 °C (room temperature) to 225 °C (just above the melting point of the PA6 phase, T_m^{PA6}). The frequency of the applied oscillations was 1 Hz and the deformation amplitude was set to 5 μm (~0.05% strain). Data were collected every 1 s. The dynamic moduli of PE at temperatures above its melting point, T_m^{PE}, were measured in plate–plate geometry in a Rheometrics RMS 800 rheometer in shear mode and then translated to tensile moduli assuming the simple relation $E^*_{tensile} = 3G^*_{shear}$.

The ternary composite materials that were made as outlined above did not flow and they could support their own weight, and preserve their original shape even at temperatures elevated above the melting point of the matrix. However, creep was observed when the sample was loaded at $T > T_m^{PE}$ (e.g. during the measurement of the modulus). To correct the value of the storage modulus for the creep, the length of the sample, $l(t,T)$, was monitored during the measurement. Assuming affine creep deformation and taking into account the constant amplitude of the oscillatory deformation, this correction is given by:

$$E^{corrected}(T) = E^{measured}(t,T)\frac{l^2(t,T)}{l^2(t_0,T_0)}$$

where t_0 and T_0 are the time and temperature at the beginning of the measurement.

3. Morphology

The morphology of the composites was examined using optical microscopy (Nikon Eclipse E600 polarizing optical microscope) and matrix dissolution techniques (e.g. Ref. [15]). Fig. 1, shows examples of the morphology of the 80/15/05 PE1/PA6/GF1 sample. The specimens for photos (a) and (b) were prepared by gently squeezing a small amount of composite material between two glass plates in a hot stage (Mettler Toledo FP 82HT) at a temperature above the melting point of the PE matrix. The specimens for photos (c) and (d) were prepared by extracting the matrix phase using boiling decalin (at $T = 180$ °C) for 3–4 days. The polyethylene matrix is removed completely under these conditions, while the rest (PA6 and GF) is not affected. In this manner the morphology of the PA6/GF structure is preserved in the same state as it is formed inside the extruder. For all ternary composites the remaining material was continuous.

Fig. 1 shows that a glass fiber network has been formed within the PE matrix. The fibers are joined ('welded') together by PA6 domains. It is apparent that only a fraction of the PA6 phase is used in the creation of these junction points. Similarly, only a part of the glass fibers is incorporated efficiently into the network. The remaining small glass fiber fragments and the free ends of the fibers, do not contribute to the PA6/GF network.

A simple theoretical model has been developed to describe the mechanical properties of the composite. It is based on a repeating unit block that represents a junction point between two glass fibers as seen in Fig. 1(d).

4. Mechanical model

The derivation of the theoretical model, proposed to describe and clarify the mechanical behaviour of the ternary composites, is discussed in details in this section. The composite is considered as consisting of a network of glass fibers inside the PE matrix. The fibers are connected together at some junction points via PA6 domains. The whole composite is thought to be an assembly of identical unit blocks centered around each junction and filling the available space.

The unit block shown in Fig. 2(a) represents a junction point of the network (Fig. 1(d)). It consists of two fibers, each of length $2l$ and radius r, connected together by a cylindrical domain of the PA6 phase with a length L and a radius a. The whole is surrounded by the PE matrix, which is also part of the block under consideration. The unit block

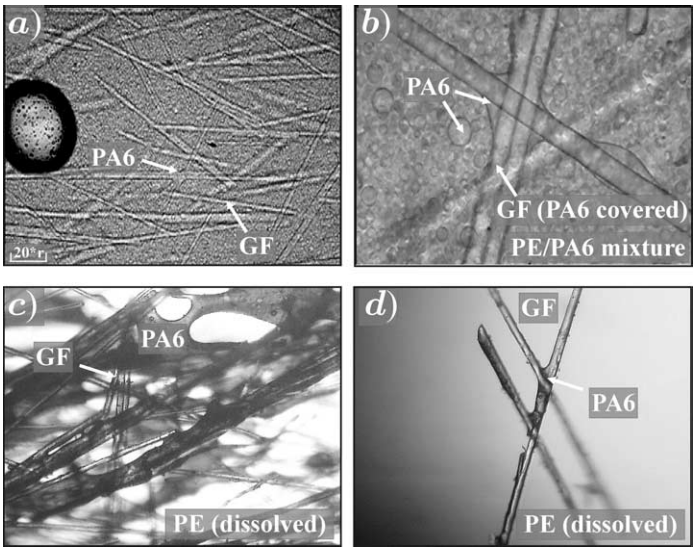

Fig. 1. Morphology images for the blend with composition 80/15/05 PE1/PA6/GF1. GF diameter 10 μm. Photos (a) and (b): the composite material was gently squeezed at 150 °C. Photos (c) and (d): the matrix phase was extracted using boiling decalin for 3–4 days.

contains some amounts of dispersed PA6 and GF that are not contributing into the network. These are expressed by their volumes V_d^{PA6} and V_d^{GF}, respectively.

The unit block is repeated in space, (Fig. 2(b)), to construct a continuous PA6/GF network. This implies that the fibers are running from side to side in the composite sample as if it is a long fiber reinforcement. Although, it looks as an oversimplification, in fact, it is quite close to the reality, where the short glass fibers are joined together by the minor PA6 phase to form an 'effectively' continuous reinforcement. Furthermore, the stress acting on every unit block is the same as the stress acting on the total sample.

Fig. 2(b), shows the initial and the strained state of the composite. The applied force, F, is transferred partially to the PA6/GF network via the cross-section of the fibers, $(2F_0)$, and partially to the PE matrix, $(F-2F_0)$. Taking into account the cross-sectional areas, the effective tensile modulus of the composite, E, can be written as the total of the weighted contributions of the network and the matrix:

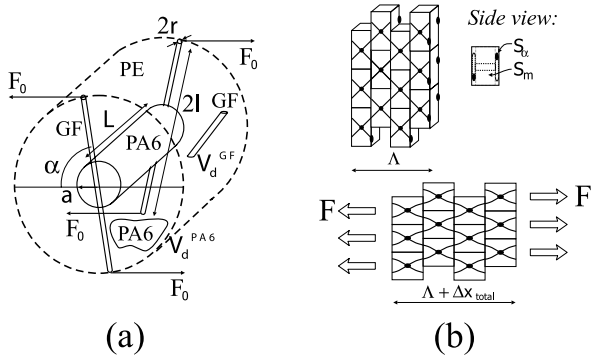

Fig. 2. Model definition. Schematic representation of one junction point and the assembly to the total composite structure.

$$E = \frac{2S_\alpha}{S_{tot}}E_0 + \frac{S_{tot} - 2S_\alpha}{S_{tot}}E_m \tag{1}$$

where $S_\alpha = \pi r^2/\cos\alpha$ is the projection of the cross sectional area of a fiber perpendicular to the external force, $S_{tot} = 4(L+4r)l\sin\alpha$ is the total cross sectional area of the unit block on which the external force acts, E_0 is the effective tensile modulus of the network structure (the junction point) and E_m is the matrix tensile modulus. The last should include the influence of the dispersed particles (loose PA6 droplets and short GF pieces) that do not participate into the network. However, this contribution is rather small, even when a substantial amount of dispersed PA6 is present in the PE phase (Fig. 4 further below), and it was neglected in the model so that $E_m \approx E_{PE}$.

Under the action of an external force, F_0, three elementary processes can occur in the network unit block: (1) the PA6-cylinder, together with the surrounding matrix can be twisted at a small angle, $\Delta\alpha$, (Fig. 3(a)); (2) the fibers can be bent at a small deflection, ξ, (Fig. 3(b)); and (3) under the action of the tensile component of the applied force, $T_{\Delta l} = F_0\cos\alpha$, the fibers can stretch, deforming in a pure tensile mode by an elongation, Δl, (Fig. 3(c)).

In the limiting case of very rigid fibers (no bending and no stretching), the force (F_0) applied on the fibers will create a force moment, $M(\Delta\alpha)$, which is related to the angle of deformation, $\Delta\alpha$, via the effective shear modulus of the unit block, G^b. Following Ref. [16]:

$$M(\Delta\alpha) = G^b\frac{\pi a^4}{L}\Delta\alpha \equiv 2F_0 l\sin\alpha \quad \text{with}$$
$$G^b = \left[G_{PA6} + G_{PE}\left[\frac{l}{a}\right]^4 - G_{PE}\right] \tag{2}$$

where $G_{PA6} \approx E_{PA6}/3$ and $G_{PE} \approx E_{PE}/3$ are the shear moduli

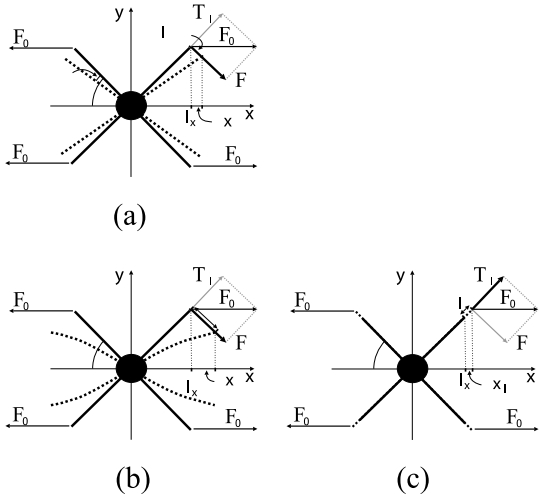

Fig. 3. Deformation modes in a junction point. Polymer twisting: (a); fibers bending: (b) and fibers stretching (c).

of PA6 and PE. The first term in the expression for G^{b} comes from the twisting of the PA6 cylinder and the other two from the twisting of the surrounding matrix.

To evaluate an effective tensile modulus of the junction due to the twisting of the polymers, E_{twisting}, we regard the junction point as an effective block of bulk material deformed under the action of the force, $2F_0$. This force is applied on the cross-sectional area, $2S_\alpha$, and results in an effective strain, $\varepsilon_\alpha = 2\Delta x_\alpha/(2l_x)$. Here, $2\Delta x_\alpha = 2l \sin\alpha\Delta\alpha$ is the effective deformation in the direction of the applied force and $2l_x = 2l\cos\alpha$ is the length of the junction element (Fig. 3(a)). Based on these considerations we have:

$$E_{\text{twisting}} = G^{b}\frac{a^4}{2Llr^2\tan^2\alpha} \tag{3}$$

The total deformation energy stored in the twisting, $U^{\text{tot}}_{\Delta\alpha}$, in terms of E_{twisting} is then given by:

$$U^{\text{tot}}_{\Delta\alpha} = 2\int_0^{\Delta\alpha} M(\Delta\alpha')\mathrm{d}\Delta\alpha' = E_{\text{twisting}}\left(\frac{2\pi r^2}{l\cos^2\alpha}\right)(\Delta x_\alpha)^2 \tag{4}$$

In the other limiting case one has only the bending of the glass fibers (no twisting of the junction point and no GF stretching). The deflection, ξ, of the fibers (Fig. 3(b)) then can be related to the force applied in the transverse direction, F_ξ. Following again Ref. [16]:

$$F_\xi \equiv F_0\sin\alpha = E_{\text{GF}}\frac{\pi r^4}{l^3}\xi \tag{5}$$

An effective tensile modulus of the junction point due to bending of the fibers only can be written, similarly to the first case:

$$E_{\text{bending}} = E_{\text{GF}}\frac{3r^2}{4l^2\tan^2\alpha} \tag{6}$$

where E_{GF} is the tensile modulus of the fibers. Adding the contributions of the four fiber parts in the unit block, the total deformation energy stored in the bending of the fibers, U^{tot}_ξ, in terms of E_{bending} becomes:

$$U^{\text{tot}}_\xi = 4\int_0^{\xi}(F_\xi)\mathrm{d}\xi' = E_{\text{bending}}\left(\frac{2\pi r^2}{l\cos^2\alpha}\right)(\Delta x_\xi)^2 \tag{7}$$

where $\Delta x_\xi = \xi\sin\alpha$ is the projection of the effective deformation, due to the bending of the fibers, in the direction of the applied force.

When only stretching of the fibers is considered (no twisting and no bending), Fig. 3(c), the effective tensile modulus of the junction point due only to the tensile deformation of the fibers will be equal to their tensile modulus, E_{GF}. Similarly to the previous cases, the expression for the total energy stored in the fiber stretching per unit block is:

$$U^{\text{tot}}_{\Delta l} = 4\int_0^{\Delta l}(T_{\Delta l})\mathrm{d}\Delta l' = E_{\text{GF}}\left(\frac{2\pi r^2}{l\cos^2\alpha}\right)(\Delta x_l)^2 \tag{8}$$

where $\Delta x_l = \Delta l\cos\alpha$ is the effective deformation in the direction of the applied force (F_0), due to the stretching of the fibers only.

In reality, all these processes occur simultaneously. Their relative extent is determined by the minimization of the total deformation energy of the unit block:

$$U^{\text{tot}} = U^{\text{tot}}_{\Delta\alpha} + U^{\text{tot}}_\xi + U^{\text{tot}}_{\Delta l} \tag{9}$$

with respect to the deformations resulting from each individual mode, and the additional constraint of constant total deformation: $\Delta x_{\text{tot}} = \Delta x_\alpha + \Delta x_\xi + \Delta x_l$.

When U^{tot} is, thus, minimized, the trade-off between the twisting, bending and stretching is established and the effective deformations resulting from this elementary modes can be expressed in terms of the effective total deformation, Δx_{tot}. Introducing Eqs. (4), (7) and (8) in Eq. (9) and minimizing gives the total deformation energy of the junction point:

$$U^{\text{tot}} = \frac{E_{\text{twisting}}E_{\text{bending}}E_{\text{GF}}}{E_{\text{GF}}E_{\text{bending}} + E_{\text{GF}}E_{\text{twisting}} + E_{\text{bending}}E_{\text{twisting}}} \times \left(\frac{2\pi r^2}{l\cos^2\alpha}\right)(\Delta x_{\text{tot}})^2 \tag{10}$$

On the other hand, the junction point can be regarded again as a block of bulk material of effective length $2l_x$. This block is deformed by the force, $2F_0$, which acts on the cross-sectional area, $2S_\alpha$. Therefore, the total deformation energy of this junction point, U^{tot}, now can be expressed by the effective tensile modulus of the junction point, E_0, and the total deformation, Δx_{tot}, as:

$$U^{\text{tot}} = \frac{1}{2}E_0 2S_\alpha 2l_x(\varepsilon)^2 = E_0\left(\frac{2\pi r^2}{l\cos^2\alpha}\right)(\Delta x_{\text{tot}})^2 \tag{11}$$

where $\varepsilon = 2\Delta x_{\text{tot}}/(2l_x)$ is the effective strain of the deformed junction point accounting for each elementary deformation

mode. Comparison of Eqs. (10) and (11) leads to the effective tensile modulus of the network:

$$E_0^{-1} = E_{\text{twisting}}^{-1} + E_{\text{bending}}^{-1} + E_{\text{GF}}^{-1} \tag{12}$$

One can see that the result is equivalent to a series addition rule for the three modes of deformation.

Some of the geometrical parameters introduced in the model can be related to the volume fractions of the components. The volumes of the glass fibers, V_{GF}, and of the PA6 component, V_{PA6}, within the total volume of the unit block, V_{total} (Fig. 2(a) and (b)), are:

$$V_{\text{GF}} = \pi r^2(4l) + V_{\text{d}}^{\text{GF}} = 4\pi r^2 l + \kappa_{\text{GF}} V_{\text{GF}},$$

$$V_{\text{PA6}} = \pi a^2 L + V_{\text{d}}^{\text{PA6}} = \pi a^2 L + \kappa_{\text{PA6}} V_{\text{PA6}},$$

$$V_{\text{total}} = (L + 4r)(4l \sin\alpha)(2l \cos\alpha)$$

$$= 8(L + 4r)l^2 \sin\alpha \cos\alpha \tag{13}$$

where $\kappa_{\text{GF}} = V_{\text{d}}^{\text{GF}}/V_{\text{GF}}$ and $\kappa_{\text{PA6}} = V_{\text{d}}^{\text{PA6}}/V_{\text{PA6}}$ denote the percentage of the GF and the PA6, respectively, that do not contribute to the network. Solving the system of Eq. (13) with respect to L and a, we get:

$$L = 4r\frac{p - \phi_{\text{GF}}(1 - \kappa_{\text{GF}})}{\phi_{\text{GF}}(1 - \kappa_{\text{GF}})}, \quad \phi_{\text{GF}} = \frac{V_{\text{GF}}}{V_{\text{total}}} \tag{14}$$

$$a = \sqrt{\frac{rl\phi_{\text{PA6}}(1 - \kappa_{\text{PA6}})}{p - \phi_{\text{GF}}(1 - \kappa_{\text{GF}})}}, \quad \phi_{\text{PA6}} = \frac{V_{\text{PA6}}}{V_{\text{total}}}$$

with $p = \pi r/(8l \sin\alpha \cos\alpha)$; ϕ_{GF} and ϕ_{PA6} are the volume fractions of the GF and PA6 phases; and $\phi_{\text{PE}} = 1 - (\phi_{\text{GF}} + \phi_{\text{PA6}})$.

Summarizing, the mechanical model consists of Eqs. (1), (3), (6), (12) and (14). The temperature dependence is introduced in the model by the temperature dependences of the tensile moduli of the polymeric components, $E_{\text{PE}}(T)$ and $E_{\text{PA6}}(T)$, while the modulus of the glass fiber reinforcement is assumed to be constant ($\approx$72 GPa).

The model has several parameters: the length $2l$ corresponds to the average distance between two junction points in the network; 2α is regarded as the average angle between two welded fibers; and κ_{PA6}, and κ_{GF} are the percentages of PA6, and GF that are not incorporated into the network structure. These four parameters can, in principle, be extracted from morphological observations.

5. Results

Figs. 4–8, compare the temperature dependences of the tensile storage modulus of composites made of different constituents and having different compositions. Some graphs also include the curves of the modulus of PA6 and PE as a reference. The storage modulus is shown, as it is more relevant for construction applications than the loss modulus.

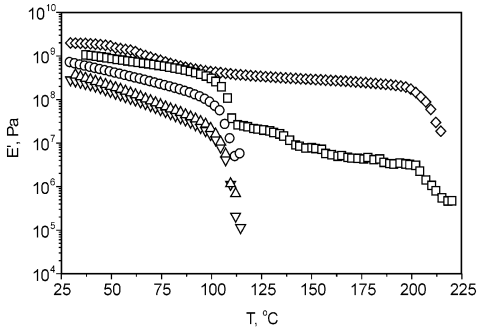

Fig. 4. Storage tensile modulus as a function of the temperature for binary and ternary composites: ◇, PA6; □, 80/15/05 PE1/PA6/GF1; ○, 95/05 PE1/GF1; △, 84/16 PE1/PA6; ▽, PE.

The first general observation from these figures is that all of the ternary composites retain relatively high values of the storage modulus, even above the melting temperature of the matrix (PE) phase. If no PA6/GF network was formed, we would expect that the whole composite would collapse above the melting point of the matrix. However, Fig. 1 shows that such network is indeed present, allowing the stress to be carried throughout the sample even after the matrix phase is molten. This results in a second 'plateau' in the storage modulus above T_{m}^{PE}. The plateau extends to the melting point of the second (PA6) component, $T_{\text{m}}^{\text{PA6}}$. Only at that point is the network destroyed and the composite collapses.

Fig. 4 demonstrates the improvement of the modulus of a binary PE/GF composite when a small amount of PA6 is added to it. Obviously, the modulus of the binary composite (95/05 PE1/GF1) is lower than the modulus of the ternary composite (80/15/05 PE1/PA6/GF1) made with the same GF loading. This difference cannot be derived from the slight increase of the matrix modulus caused by the presence of a dispersed PA6 phase. The figure includes the modulus of a PE/PA6 binary blend prepared in the same proportion as in the ternary blend, namely: 84/16 PE1/PA6. Therefore, the

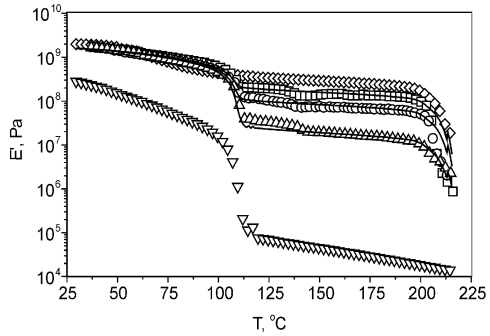

Fig. 5. Influence of the PA6 volume fraction on the storage tensile modulus of PE1/PA6/GF1 composites: ◇, PA6; □, 65/25/10 PE1/PA6/GF1; ○, 75/15/10 PE1/PA6/GF1; △, 85/05/10 PE1/PA6/GF1; ▽, PE. Solid lines represent the theoretical fits, see the fitting details included in Table 2.

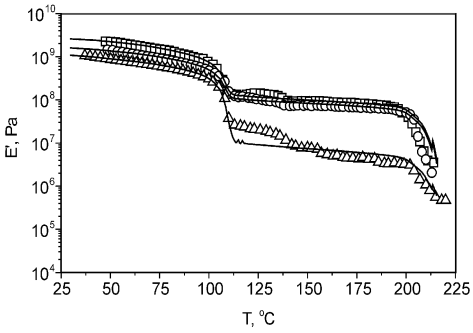

Fig. 6. Influence of the GF volume fraction on the storage tensile modulus of PE1/PA6/GF1 composites: □, 70/15/15 PE1/PA6/GF1; ○, 75/15/10 PE1/PA6/GF1; △, 80/15/05 PE1/PA6/GF1. The solid lines represent the model fits.

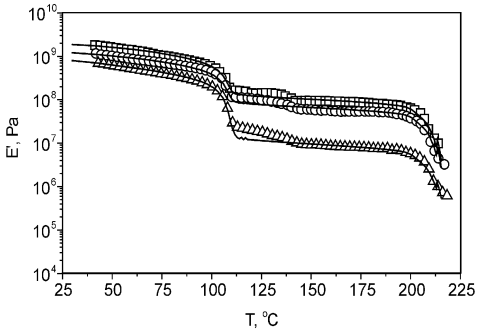

Fig. 8. Influence of the GF volume fraction on the storage tensile modulus of PE2/PA6/GF1 composites: □, 70/15/15 PE2/PA6/GF1; ○, 75/15/10 PE2/PA6/GF1; △, 80/15/05 PE2/PA6/GF1. The solid lines are the model fits.

enhanced value of the modulus in the ternary composite has to be attributed to the apparent increase of the fibers length due to their 'welding' together by the minor PA6 component in a reinforcing network. Furthermore, the second 'plateau' of the modulus at temperatures above the T_m^{PE} is absent in all binary composites.

Fig. 5 shows the modulus of the ternary composites as a function of the PA6 amount at constant fiber volume fraction. These graphs reveal that the modulus of the ternary composites below the T_m^{PE} is almost independent of the amount of the PA6, at least for $\phi_{PA6} \geq 5$ vol%. Above the melting point of the PE, however, the samples containing more PA6 show higher values of the storage modulus. Apparently, the increase of the amount of the PA6 phase improves the quality of the effective (PA6/GF) network either by increasing the volume of the PA6 at the junction points or by creating new junctions. Therefore, the torsional stiffness of a junction point and the apparent length of the fibers involved in the stress transfer increases, enhancing the tensile modulus of the composite.

The effect of varying the GF loading at constant PA6 volume fraction, is shown in Fig. 6. A difference in the tensile modulus can be seen in the whole measured temperature region. As it might be expected, the fibers reinforce equally well both at temperatures below and above the matrix melting point. On the other hand, varying the amount of the PA6 component influences the 'effective' length of the fibers and the network strength but does not change the total amount of the reinforcement. This becomes more important after the matrix is molten, when the stress is transfered only by the fiber network. Therefore, the effect of the presence of PA6 is more pronounced above T_m^{PE}.

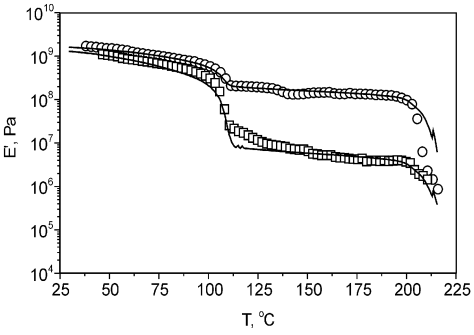

Fig. 7. Comparison of the storage tensile modulus, polyamide (GF1) vs. polyethylene (GF2) compatible fibers: ○, 65/25/10 PE1/PA6/GF1; □, 65/25/10 PE1/PA6/GF2. The solid lines represent the model fits.

The influence of the interfacial properties of the components is demonstrated in Fig. 7. The storage moduli of the 65/25/10 PE1/PA6/GF1 and 65/25/10 PE1/PA6/GF2 composites prepared using the same amounts of, respectively, polyamide and polyethylene compatible glass fibers are shown. The compatibility of the glass fibers with the minor polymeric component (PA6) turns out to be the most important parameter governing the mechanical properties. The composites made of PA6 compatible GF1 have much higher tensile modulus than the one with the PE compatible GF2. This difference is most pronounced above T_m^{PE}, where the modulus of the GF1 composite is an order of magnitude higher than the modulus of the composite with GF2.

In order to understand this result one needs to consider the manufacturing of the composites. The surface properties of the glass fibers influence the wetting kinetics during the processing step and, therefore, control the formation of the PA6/GF network. That is, fewer junctions will be created in the case of the PE compatible GF2, and a looser network will result because of the reduced tendency of the PA6 to migrate and spread on the GF2 surface. On the other hand, the surface properties of the glass fibers also determine the stability of the already formed network. Therefore, even if the formation of the network (in the GF2 case) is completed to a certain extent during the extrusion process, this network could deteriorate later in the next preparation step, the hot-press consolidation of the samples, by the displacement of the PA6 component away from glass fiber surface and the junction points.

The influence of the viscosity of the matrix was also investigated. Fig. 8, shows some of the data for the samples prepared using the higher viscosity polyethylene (PE2). One might expect that a matrix with higher viscosity would cause slower wetting kinetics and incomplete network

formation during the blending. This should result in a lower modulus. However, very little influence of the viscosity of the PE on the tensile modulus of the composites can be seen (compare Figs. 6 and 8). The data suggest that in the forced flow within the extruder the wetting of the fibers by the minor phase is not affected by the viscosity of the matrix. Another possible reason may be that the incompleteness of the network in the case of the PE2 matrix is compensated by a better orientation of the fibers along the flow direction in the higher viscosity medium.

Figs. 5–8 also show the results of the mechanical model. It can be seen that the model can describe most of the curves rather well. These results are discussed in the following section.

6. Discussion

6.1. The fit of the data by the model

Some fits of the experimental data are shown in Figs. 5–8. A summary of the model parameters for all measurements is given in Tables 2 and 3. In these calculations it was assumed that all fibers participated in the PA6/GF network, i.e. $\kappa_{GF}=0$. This assumption is quite plausible for two reasons. First, the morphology images (Fig. 1) show that very few short GF pieces are not incorporated into the PA6/GF network. Second, every fiber takes part in several junction points. Therefore, the importance of the free ends, which do not contribute to the network, can safely be neglected in comparison to the total fiber length. Thus, only three parameters: l, α and κ_{PA6} are left to be evaluated by fitting to the data. The influence of these parameters on the predictions of the model is discussed further down in this section (Section 6.2). The radius a and the length L of the PA6 cylinder, as well as the number of junction points, N, or the inverse of the unit block volume, were calculated from these three parameters.

An idea about the order of magnitude of the geometrical parameters l and α can be obtained from the morphology shown in Fig. 1: $l\approx 50$ μm and $\alpha\approx 15°$. These values are in the same order of magnitude as the corresponding values evaluated by fitting the modulus data (Table 2).

When the PA6 content increases at constant GF loading the relative amount of the PA6 incorporated into the network, $1-\kappa_{PA6}$, decreases. The absolute amount of PA6 still involved into the network $\phi_{PA6}(1-\kappa_{PA6})$, however, increases. In terms of the other model parameters this increase means higher values of the radius, a, and the volume of the PA6 cylinder connecting the glass fibers. The distance between the junction points is independent of the amount of PA6: $l\approx 41$ μm for GF1 and $l\approx 47$ μm for GF2. The average distance, $2l$, between two neighbouring junction points and the length, L, of the PA6 cylinder connecting the fibers are determined completely by the spatial distribution of the fibers and, therefore, only by the fiber volume fraction and the processing conditions. The fits in the case of the PE compatible fibers, GF2, reveal that a smaller fraction of PA6 participates in the junction points than when the PA6 compatible fibers, GF1, are used.

Analysing the data for the composites having different GF volume fractions at constant PA6 content, a clear trend in the values of l can be observed. When the GF content increases the total number of the junction points, N, also increases. The expected scaling (in its upper limit) for 3D random fiber distribution should be $N\sim\phi_{GF}^2$, while we obtained $N\sim\phi_{GF}^{4/3}$ after the fitting. This scaling is reasonable, given our approximations, and it means that not every crossing of two fibers is a network junction point. The average distance along a fiber between two junction points, therefore, is a decreasing function of the GF volume fraction: $l\sim\phi_{GF}^{-1/3}$. Although, it is not very pronounced, it seems that if the content of the GF increases, the amount of the PA6 not incorporated into the network also increases. This indicates that by increasing the amount of GF, a larger number of weaker junctions are created, while the increase of the amount of PA6 does not change the number of the junction points noticeably but makes them stiffer.

Table 2
Parameters of the model to fit the PE1-based composites

PA6-compatible GF	α (°)	l, μm	κ_{PA6}	$\phi_{PA6}(1-\kappa_{PA6})$ (%)	a, μm	L, μm	N, mm^{-3}
65/25/10 PE1/PA6/GF1	11.5	41	0.40	15.00	14.60	29	7764
75/15/10 PE1/PA6/GF1	11.5	41	0.40	10.50	12.20	29	7764
85/05/10 PE1/PA6/GF1	11.5	41	0.05	4.75	8.19	29	7764
70/15/15 PE1/PA6/GF1	12.0	35	0.54	6.90	9.80	29	13642
80/15/05 PE1/PA6/GF1	8.0	53	0.58	6.30	8.73	29	3003
PE-compatible GF	α (°)	l, μm	κ_{PA6}	$\phi_{PA6}(1-\kappa_{PA6})$ (%)	a, μm	L, μm	N, mm^{-3}
65/25/10 PE1/PA6/GF2	14.5	47	0.87	3.25	8.77	37	3608
75/15/10 PE1/PA6/GF2	14.5	47	0.87	1.95	6.80	37	3608
85/05/10 PE1/PA6/GF2	14.5	47	0.87	0.65	3.90	37	3608
70/15/15 PE1/PA6/GF2	23.0	41	0.98	0.30	5.10	59	6205
80/15/05 PE1/PA6/GF2	8.0	59	0.84	2.40	5.90	154	1437

Table 3
Parameters of the model to fit the PE2-based composites

PA6-compatible GF	α (°)	l, μm	κ_{PA6}	$\phi_{PA6}(1-\kappa_{PA6})$ (%)	a, μm	L, μm	N, mm^{-3}
65/25/10 PE2/PA6/GF1	10.0	40	0.05	23.75	15.90	37.4	7958
75/15/10 PE2/PA6/GF1	14.5	40	0.52	7.20	11.90	20.5	7958
85/05/10 PE2/PA6/GF1	12.0	40	0.05	4.75	8.20	28.3	7958
70/15/15 PE2/PA6/GF1	16.0	33	0.70	4.50	9.98	9.9	14469
80/15/05 PE2/PA6/GF1	11.0	50	0.55	6.75	10.30	63.9	3183
PE-compatible GF	α (°)	l, μm	κ_{PA6}	$\phi_{PA6}(1-\kappa_{PA6})$ (%)	a, μm	L, μm	N, mm^{-3}
65/25/10 PE2/PA6/GF2	10.5	46	0.55	11.25	12.50	62.0	3687
75/15/10 PE2/PA6/GF2	12.0	46	0.75	3.75	7.94	51.4	3687
85/05/10 PE2/PA6/GF2	17.0	46	0.80	1.00	5.73	29.9	3687
70/15/15 PE2/PA6/GF2	12.5	42	0.78	3.30	7.87	28.0	6057
80/15/05 PE2/PA6/GF2	10.0	58	0.74	3.90	8.37	121.0	1462

To conclude, three of the parameters of the proposed model were needed to fit the experimental data. The parameters have a well-defined physical meaning. The order of magnitude of their values obtained after fitting of the storage dynamic tensile modulus agree with the morphological observations. The description of the experimental data by the model is rather good.

6.2. Parametric study of the model

When the fibers are perfectly oriented along the loading direction, i.e. when $\alpha \to 0°$, the presence of the PA6 phase is of no importance. Because the fibers are long enough, using our model we, then, expect the modulus of the composite to be given by a parallel mixing rule similar to perfectly aligned continuous reinforcement:

$$E(\alpha \to 0°) = \phi_{GF}E_{GF} + (1 - \phi_{GF})E_m \quad (15)$$

At the other limit $\alpha \to 90°$ the model predicts a somewhat lower value than the matrix modulus, E_m:

$$E(\alpha \to 90°) = (1 - \phi_{GF})E_m \quad (16)$$

Although, in this limit all the fibers are aligned perpendicular to the loading direction ($2\alpha = 180°$) one still expects that the fibers will provide some reinforcement. The prediction of the model, obviously, fails. In terms of the model geometry, the failure originates from the impossibility to spatially accommodate the fibers and still ensure the existence of the network in this limiting case. This means that the model cannot incorporate the reinforcing abilities of loose short fibers correctly and should not be used for such composites.

The effect of the angle between the fibers, α, on the predicted modulus, is shown in Fig. 9, where the other parameters remain constant. The influence of α is different at temperatures below and above the melting point of the matrix polymer. Below T_m^{PE}, e.g. at 50 °C, when α is increased, the predicted modulus smoothly drops from the value from Eq. (15). When α approaches 90°, E levels off at a value close to the matrix modulus, E_m (50 °C), (Eq. (16)). In the region above T_m^{PE}, e.g. at 150 °C, an increase of α initially results in a very rapid decrease of the modulus (a few orders of magnitude within 1° as seen in the logarithmic plot of Fig. 9), followed by a slow increase. The predicted modulus passes through a local maximum and then it decreases to a level close to the matrix modulus, E_m (150 °C) as $\alpha \to 90°$ (Eq. (16)).

This complex behaviour is a direct result of the competition between all the elementary deformation modes considered in the model. At very low values of the angle α ($\alpha \to 0°$) the twisting of the polymers and the bending of the fibers are too expensive to take place. The dominant mode of deformation then is the tensile deformation of the fibers, and the composite modulus is governed by the tensile modulus of the fibers (Eq. (15)). Upon increase of α the twisting mode becomes the easiest deformation mode and the modulus of the composite drops. The decrease is moderate at the temperatures below T_m^{PE} and very rapid at the temperatures above T_m^{PE}, where the very low matrix modulus results in a very low $E_{twisting}$. At intermediate values of the angle α the bending of the fibers becomes the most favourable deformation mode and it dominates the composite modulus. The cross-over of $E_{twisting}$ and $E_{bending}$ corresponds to the maximum in the $E(\alpha)$ curve at $T_2 = 150$ °C (Fig. 9). At very large angles the twisting mode prevails again but the effective network modulus, E_0, is so small that the composite modulus becomes dominated entirely by the modulus of the matrix (Eq. (16)).

The gap in the curves in Fig. 9 point out that there is no solution provided by the model for some values of the angle α. The lack of a solution, for this values of the angle α, stems from the impossibility to accommodate the fibers within the volume of the chosen unit block (Fig. 2) and for the chosen values of the other model parameters (particularly l and ϕ_{GF}). In fact, for a fixed fiber loading, ϕ_{GF}, and

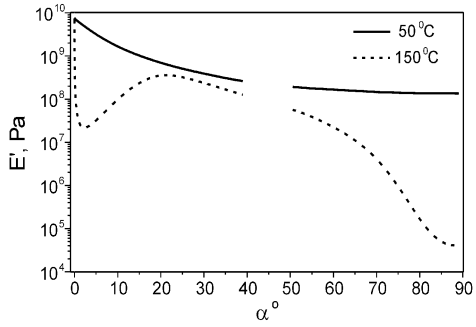

Fig. 9. Variation in the composite modulus, E, with α, i.e. the fiber orientation. The other model parameters are constant: $l=40$ μm, $\kappa_{PA6}=0$, $\kappa_{GF}=0$; the composition is 75/15/10 PE1/PA6/GF1. The changes are shown for two different temperatures: (—) below the melting point of the matrix phase ($T_1=50$ °C); (- - -) above the melting of the matrix phase ($T_2=150$ °C).

angle, α, there is an upper limit of the possible values of l (as it follows from Eq. (14)). Similarly, not all combinations of l, ϕ_{GF} and α are permitted for steric reasons.

The influence of the length between two junction points, $2l$, on the composite modulus, $E(l)$, at the two fixed temperatures ($T_1=50$ °C and $T_2=150$ °C) is shown in a linear plot in Fig. 10. As l increases, the composite modulus also increases up to a local maximum. The maximum is reached at a lower value of l for the plot corresponding to the lower temperature ($T_1=50$ °C).

This behaviour can be explained again by the competition between the elementary deformation modes. At very low values of l it is very difficult to bend and elongate the fibers. The dominant deformation mode, then, is the twisting of the polymers. For $l\rightarrow 0$, however, this deformation mode results in such low values of the effective network modulus, E_0, that the total composite modulus becomes determined by the modulus of the matrix. With the increase of the length l the twisting mode becomes more 'expensive' (larger volumes of polymers are becoming involved), whereas the bending of the fibers is facilitated. The maximum of $E(l)$ is obtained at the cross-over between $E_{twisting}$ and $E_{bending}$. The larger value of $E_{twisting}$ at the temperatures under T_m^{PE} leads to the earlier positioning of the maximum in the predicted composite modulus for $T_1=50$ °C (Fig. 10).

The effect of the parameter κ_{PA6} is simpler. An increase of κ_{PA6} reduces the level of the modulus because it reduces the volume of the connecting PA6 cylinder at the junction points. This is more pronounced above the melting point of the matrix phase than below (Fig. 11) because the importance of the presence of PA6 is greater in the absence of a supporting matrix. The variations of the modulus below T_m^{PE} are an order of magnitude smaller than the changes above T_m^{PE}.

One may notice that even when all of the PA6 phase is completely removed from the network and exists only as a dispersed phase ($\kappa_{PA6}=1$), i.e. when a true network does not exist any more, the model still predicts rather high values for the modulus, particularly, in the region below the melting point of the matrix. This is of course unrealistic, it stems from the fact that the fibers are considered to stay 'pinned' at the junction point. In reality, if there is no PA6 phase providing the contact between the fibers, all the elementary modes involved in the deformation of a junction point will become inactive and the modulus of the composite will be the same as the modulus of a short fiber reinforced polymer. Therefore, the proposed model is inaccurate when very low PA6 volume fractions are considered. For the amounts of PA6 used in this work, however, the model is undoubtedly appropriate and, if the blend morphology is known, one should be able to predict the composite modulus correctly.

7. Conclusions

An improvement of the mechanical properties of short glass fiber composites (PE/GF) was achieved after addition of minor quantities of a second thermoplastic polymer (PA6). Unexpectedly high values of the tensile modulus of the ternary composites (PE/PA6/GF) were measured well above the melting point of the matrix phase. The morphology investigation revealed the existence of a fiber network (PA6/GF) within the matrix polymer (PE). The network formation process is governed by the wetting of the fiber surface by the minor thermoplastic component (PA6). The modulus of the composites made of glass fibers that have been treated to be compatible with the minor component (PA6) is an order of magnitude higher than the one of the composites made with matrix compatible glass fibers. An increase in the amount of GF results in an increase of the tensile modulus of the composites in the whole temperature range up to the melting point of the minor polymeric phase (PA6). An increase in the amount of PA6 results in a substantial increase of the modulus of the composite at temperatures above the melting point of the matrix polymer. The viscosity of the PE matrix has no significant influence on the composite modulus. A model for the mechanical properties of the ternary composites has been developed based on the existence of the PA6/GF

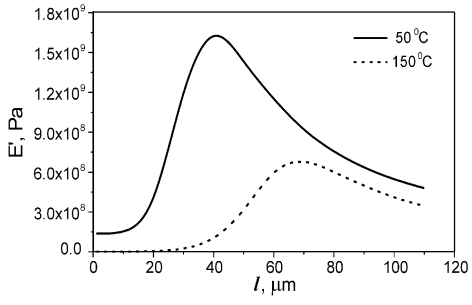

Fig. 10. Variation in the composite modulus, E, with the length l, i.e. half the distance between two neighbouring junction points, for the 75/15/10 PE1/PA6/GF1 composite, at temperatures below the melting point of the matrix phase (—, $T_1=50$ °C), and above it (- - -, $T_2=150$ °C). The other model parameters are constant: $\alpha=10°$, $\kappa_{PA6}=0$, $\kappa_{GF}=0$.

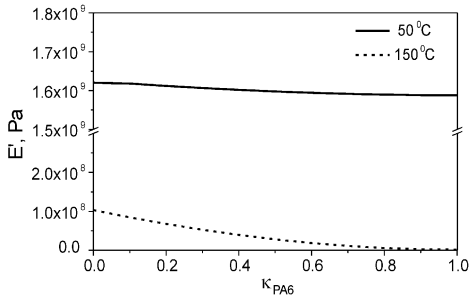

Fig. 11. Variation in the composite modulus, E, with κ_{PA6}, i.e. the fraction of the PA6 phase not incorporated into the network, for the 75/15/10 PE1/PA6/GF1 composite, at temperatures below the melting point of the matrix phase (—, $T_1=50$ °C), and above it (- - -, $T_2=150$ °C). The other model parameters are: $l=40$ μm, $\alpha=10°$, $\kappa_{GF}=0$.

network. The model gives a proper description of the measured storage dynamic tensile modulus of the manufactured composites in the whole temperature range and uses physically well defined fitting parameters.

Acknowledgements

We would like to thank Prof J.J. Elmendorp for the initial idea and for his continuous input on this project; PPG Industries for their kind support of this work by the delivery of the glass fibers. The work of P.G. Malchev, A.D. Gotsis and S.J. Picken forms part of the research programme of the Dutch Polymer Institute, project number 256. In addition C.T. David acknowledges the ERASMUS Exchange Program for the financial support.

References

[1] Grace HP. Chem Eng Commun 1982;14:225–77.
[2] Enikolopyan NS, Fridman ML, Stalnova IO, Popov VL. Adv Polym Sci 1990;96:1–67.
[3] Xanthos M, Narh KA. Polym Compos 1998;19(6):768–80.
[4] Tchoudakov R, Breuer O, Narkis M. Polym Eng Sci 1996;36(10):1336–46.
[5] Maeng YJ, Yoon SB, Suh MH, Im WB, Lee SH. Polym Compos 2000;21(1):41–50.
[6] Fisher I, Zoldan J, Siegman A, Narkis M. Polym Compos 2000;21(2):476–91.
[7] Fisher I, Siegman A, Narkis M. Polym Compos 2002;23(3):464–77.
[8] Noh C-H, Yoon BS, Suh MH, Lee SH. Polymer 2001;42(6):2695–700.
[9] Coran AY, Patel R. J Appl Polym Sci 1976;20:3005–16.
[10] Heinrich G, Klüppel M. Adv Polym Sci 2002;160:1–44.
[11] Gavin AB, Balazs AC. Mol Simul 2004;30(4):249–57.
[12] Åström J, Saarinen S, Niskanen K, Kurkijärvi J. J Appl Phys 1994;75(5):2383–92.
[13] Åström J, Mäkinen JP, Alava MJ, Timonen J. Phys Rev E 2000;61(5):5550–6.
[14] Levine AJ, Head DA, MacKintosh FC. J Phys: Condens Matter 2004;16:S2079–S88.
[15] Willemse RC, Posthuma de Boer A, van Dam J, Gotsis AD. Polymer 1998;39:5879–87.
[16] Feynman RP, Leighton RB, Sands M. The Feynman lectures on Physics. vol. 2. London: Addison-Wesley Publishing Company; 1964 [chapter 38].